frontiers | Frontiers in Chemistry

TYPE Original Research
PUBLISHED 22 July 2022
DOI 10.3389/fchem.2022.947052

OPEN ACCESS

EDITED BY
Shijie Li,
Zhejiang Ocean University, China

REVIEWED BY
Yanping Liu,
Zhejiang Ocean University, China
Xiaofeng Shen,
Zhejiang University of Science and Technology, China

*CORRESPONDENCE
Nengmei Deng,
353350107@qq.com

SPECIALTY SECTION
This article was submitted to Photocatalysis and Photochemistry, a section of the journal Frontiers in Chemistry

RECEIVED 09 June 2022
ACCEPTED 27 June 2022
PUBLISHED 22 July 2022

CITATION
Zhao J and Deng N (2022), TiO_2 NPs/h-BN: Preparation and catalytic activities of a novel AP catalyst.
Front. Chem. 10:947052.
doi: 10.3389/fchem.2022.947052

TiO_2 NPs/h-BN: Preparation and catalytic activities of a novel AP catalyst

Jun Zhao and Nengmei Deng*

West Anhui University, Lu'an, China

The thermal decomposition performance of an oxidizer directly determines the thrust and specific impulse properties of the solid propellant. Hexagonal boron nitride (h-BN) has the characteristics of high catalytic activity and good stability, which can improve the heat release and decomposition temperature of the oxidant, and then improve the energy performance of the propellant. In this study, a novel hybrid material TiO_2 NPs/h-BN was successfully prepared by *in situ* growth, and it was found that when 5 wt.% TiO_2 NPs/h-BN was added, the initial decomposition temperature of ammonium perchlorate (AP) decreased by 67.6°C. Due to the addition of TiO_2, the gap between the h-BN layers as well as the specific surface increased, which optimized its thermocatalytic performance, and it also proposed a catalytic mechanism for the thermal decomposition process of AP.

KEYWORDS

TiO_2 NPs/h-BN, AP, BN, thermal decomposition, catalytic

Introduction

Solid propellants consisted of oxidants, binders, metal burners, and other additional components. Among them, the oxidant, as the source of oxygen required for propellant combustion, occupied more than 70% of the propellant, and its thermal decomposition performance had a great influence on the combustion of the propellant. Among these oxidants, AP had the advantages of high effective oxygen content and high density and was one of the most commonly used oxidants in solid propellants (Li et al., 2021). However, the properties of AP, such as high thermal decomposition temperature, high reaction activation energy, low heat release, and non-concentrated heat release, were important factors restricting the development of high-energy solid propellants (Huang et al., 2021). Therefore, in order to meet the needs of modern aerospace technology and the world arms race for high-energy solid propellants, it is necessary to improve the thermal decomposition performance of AP (Li et al., 2020a).

Recently, two-dimensional atomic crystals are now attracting increasing attention in various fields and applications, inspired by the "graphene gold rush" (Sun et al., 2018; Li et al., 2020b; Shen et al., 2021a; Shen et al., 2021b; Li et al., 2022). As a typical graphene-like material, h-BN has attracted great research interest because of its good oxidation resistance up to 850°C, excellent acid chemical stability, high thermal conductivity, excellent elastic modulus, and good mechanical flexibility (Sun et al., 2016). More

importantly, h-BN has been identified as a promising dielectric layer or protective encapsulation material (Li et al., 2012; Shen et al., 2020; Wang et al., 2020). Metal oxide semiconductor materials had the advantages of heat resistance, antitoxicity, photosensitivity, heat sensitivity, and impurity sensitivity and were suitable for modulation, so they have attracted much attention in the field of catalysis (Thomas et al., 2016; Zhu et al., 2016; Li et al., 2017; Li et al., 2020c). Therefore, we propose a technical scheme for the preparation of novel composite catalysts using few-layer boron nitride–supported TiO_2 (Medvecká et al., 2018).

In this work, we first used a purely physical green peeling method—liquid nitrogen impact method to peel off the multilayer boron nitride (BN)—and then used a one-step synthesis *in situ* growth method to obtain the target product TiO_2 NPs/h-BN, and the thermal catalytic effect of the composite on AP was studied. The results showed that the decomposition temperature of ammonium perchlorate decreased by 67.6°C when 5% (mass fraction) was added. Also, the catalytic mechanism was studied.

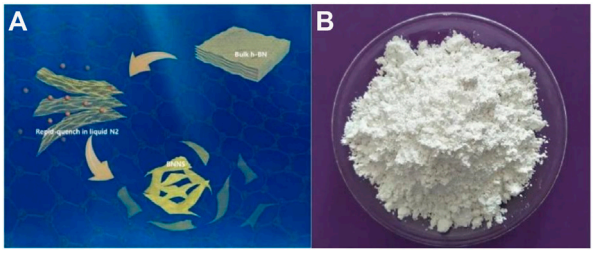

SCHEME 1
(A) Gas exfoliation of h-BN triggered by thermal expansion.
(B) Photograph of TiO_2 NPs/h-BN.

Experimental

Chemicals and apparatus

Ammonium chloride (99%), aluminite powder (99.99%), BBr_3 (AR), hydrochloric acid (35%), ethanol, glacial acetic acid, butyl titanate, and AP (AR) were obtained from Aladdin (Shanghai, China).

Preparation of h-BN

Synthesis experiments were performed in a N_2-flow glove box. NH_4Cl (0.150 mol), Al (0.100 mol), and BBr_3 (0.050 mol) were put into a stainless steel autoclave with a volume of 50 ml. The autoclave was sealed and heated in an oven at a ramp rate of 10°C/min from room temperature to 500°C and held at 500°C for 10 h (Huang et al., 2018). The product was dried under vacuum at 80°C for 10 h.

Preparation of h-BNNS

The prepared 5 g of white powder was weighed, placed in a crucible, placed in a muffle furnace, heated to 800°C at a heating rate of 10°C, and kept warm for 30 min. At the end of heat preservation, it was quickly taken out, poured into the prepared liquid nitrogen (L-N_2) until the L-N_2 gasified completely. The white powder was suddenly cooled, liquid nitrogen was rapidly evaporated, and the steam-impinging boron nitride powder was boiled. The essence of this strategy lies in the combination of a high temperature–triggered expansion of bulk h-BN and a subsequent L-N_2 gasification that exfoliates the h-BN (Li et al., 2019). Repeat the aforementioned steps three times to obtain the target product (h-BNNS). Scheme 1A was gas exfoliation of h-BN triggered by thermal expansion, and Scheme 1B was the photograph of TiO_2 NPs/h-BN.

Preparation of TiO_2 NPs/h-BN

A volume of 5.0 ml ethanol and 2.0 ml of glacial acetic acid were placed in a beaker, then 6.8 ml of butyl titanate was added to it, and at 30°C, under magnetic stirring for 10 min, 0.8 g of h-BNNS was added and labeled as Solution A (Li et al., 2018). Into another beaker was added 4.0 ml of deionized water, 5.0 ml of ethanol, and 7.2 ml of glacial acetic acid and magnetically stirred for 10 min to uniformly mix to obtain Solution B (Xue et al., 2011). After the dropwise addition was completed, stirring was continued for 20 min to obtain a uniform solution. It was allowed to stand at room temperature for 24 h to form a gel and dried in a drying oven at 80°C for 12 h. The ground samples were placed in a muffle furnace, calcined at 400°C for 2 h, and then cooled naturally to obtain TiO_2 NPs/h-BN.

Results and discussion

Sample characterization

The FT-IR result is shown in Figure 1A. The two absorption peaks at 1388.6 cm^{-1} and 813.4 cm^{-1} are the in-plane stretching vibration of B-N and the out-of-plane bending B-N-B vibration, respectively. The absorption peak at 3433.8 cm^{-1} is the in-plane stretching vibration of N-H (Thomas et al., 2008). The Raman spectrum showed that the G-band frequency of h-BNNS was shifted up relative to that of bulk h-BN (1366.8 cm^{-1} vs. 1365.8 cm^{-1}; Figure 1B). The G-band shift could be attributed

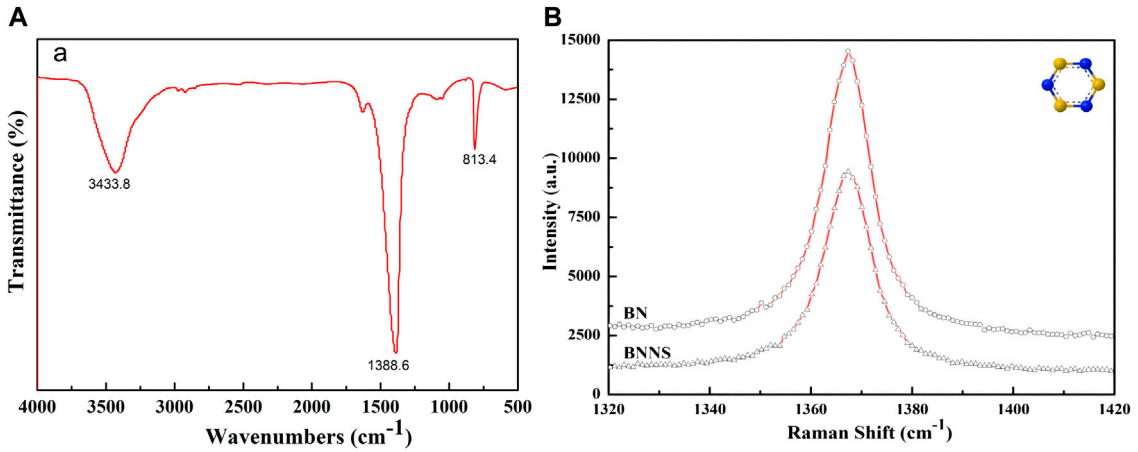

FIGURE 1
(A) FT-IR spectra of h-BN. **(B)** Raman characterizations of bulk h-BN and h-BNNS.

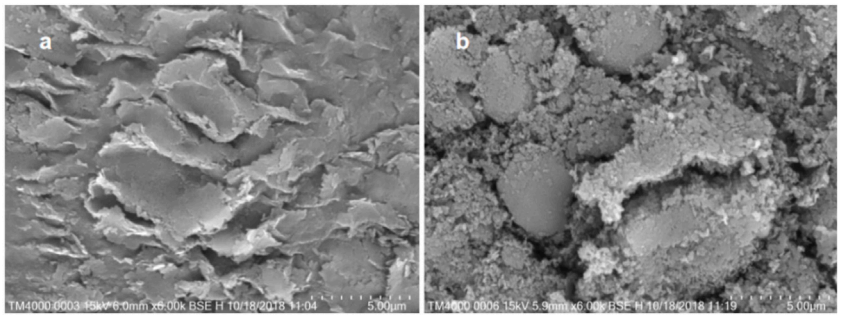

FIGURE 2
Characterization of exfoliated h-BNNS. **(A)** SEM of h-BN. **(B)** SEM of h-BNNS.

to the reduction of h-BN layers, which led to higher in-plane strain and weaker interlayer interactions.

As shown in Figure 2, the scanning electron microscope images of the parent h-BN and h-BNNS are shown in Figures 2A,B. Compared with the bulky h-BN precursors, h-BNNS was much smaller in size and possessed nanosheet-like morphology (Lei et al., 2018).

The SEM results also proved that we successfully prepared TiO_2 NPs/h-BN, as shown in Figure 3. TiO_2 NPs were uniformly dispersed on the surface of the h-BN (Hosseini et al., 2018). In addition, EDS showed that TiO_2 was uniformly distributed on boron nitride nanoparticles.

Figure 4 shows the TEM of TiO_2 NPs/h-BN. We found that TiO_2 had microspherical morphology, and the outer layer was covered by h-BN. It was consistent with the SEM characterization results.

Figure 5A shows the XPS of TiO_2 NPs/h-BN. The characteristic peaks at 458.9 and 464.7 eV correspond to the binding energies of Ti 2p1/2 and Ti 2p3/2, respectively, indicating that Ti was at positive 4 valence, Ti^{4+}. Nitrogen adsorption/desorption isotherms were conducted at 77 K to study the textural properties of TiO_2 NPs/h-BN (Figure 5B). Because of its spherical structure, its specific surface area was large. Based on the nitrogen adsorption and desorption curves, the BET surface areas of TiO_2 NPs/h-BN was 112.5 $m^2\ g^{-1}$.

Catalytic activities of TiO_2 NPs/h-BN in the thermal decomposition of AP

In order to fully demonstrate the effectiveness of TiO_2 NPs/h-BN in catalyzing the thermal decomposition of AP, we carried

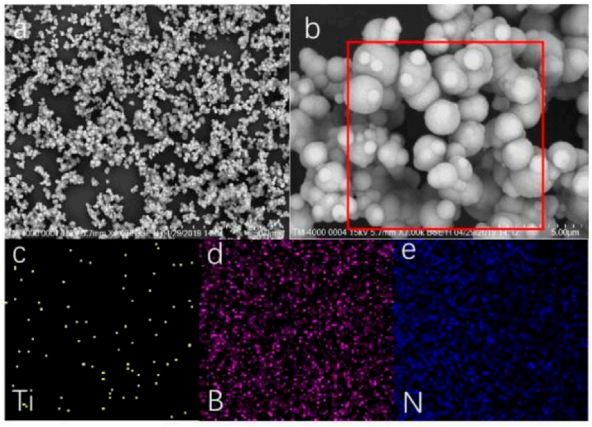

FIGURE 3
SEM of TiO_2 NPs/h-BN **(A,B)** and EDS of TiO_2 NPs/h-BN **(C–E)**.

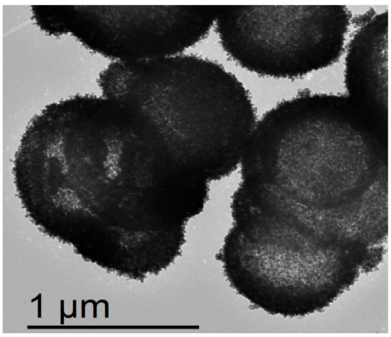

FIGURE 4
TEM of TiO_2 NPs/h-BN

out research work by means of thermal analysis. As shown in Figure 6A, compared with the DTA curve of pure AP, the decomposition peak temperature of AP was advanced to 395.7°C by the catalysis of TiO_2. After the addition of TiO_2 NPs/h-BN, the HTD temperature was further advanced to 380.8°C, confirming the intrinsic catalytic effect of TiO_2 NPs/h-BN on AP. This conclusion is also confirmed by the TGA-DTG results, as shown in Figure 5B; in the TGA curve of AP, the two characteristic weight loss steps correspond to the LTD and HTD phases where the weight loss rate reaches 25% and 74%, respectively (Jacobs and Russell-Jones, 1968; Morales- Verdejo et al., 2018; Yuan et al., 2018).

As shown in Figure 7, we collected samples before and after thermal catalysis and performed by XRD. Diffraction peaks existed in all samples: 2θ = 25.5°, 37.8°, 48.2°, 53.7°, 55.2°, 62.6°, 68.9°, 70.4°, and 75.3°, which corresponding to this diffraction peak was (0002), (004), (112), (200), (0004), (204), (116), (220), and (215); these diffraction peaks were compared with h-NB and TiO_2. We collected the catalytic effect and recovery rate of the TiO_2 NPs/h-BN after two cycles of thermocatalysis in Table 1.

Catalytic mechanisms

The addition of h-BNNS inhibited the agglomeration of TiO_2 particles during the preparation process and synergistically enhanced the catalytic activity by forming a hybrid structure (Al- Ani and Hogarth, 1985; Al- Kuhaili et al., 2002; Cui et al., 2012; Xu et al., 2013; Zhao et al., 2016). The catalytic effect of h-BN was attributed to the negatively charged h-BN surface (Shen et al., 2006; Tu et al., 2014), which facilitated the transfer of induced holes to the TiO_2 surface due to the electrostatic attraction between them to form OH^- or ·OH radicals, which

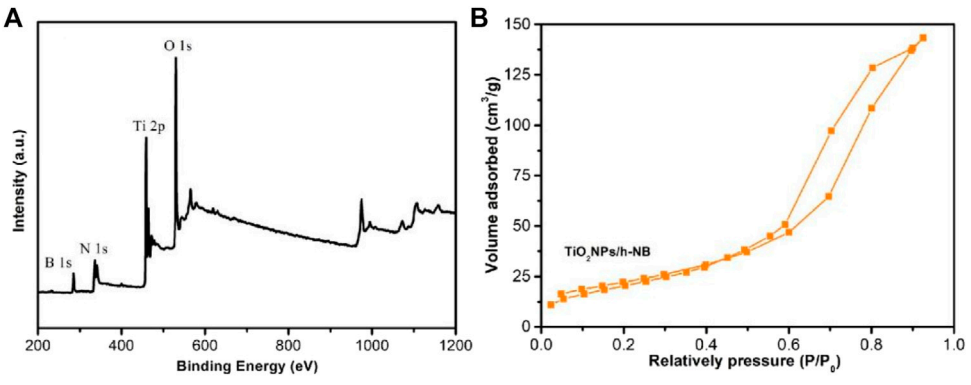

FIGURE 5
(A) XPS of TiO_2 NPs/h-BN. **(B)** N2 adsorption/desorption isotherms of TiO_2 NPs/h-BN.

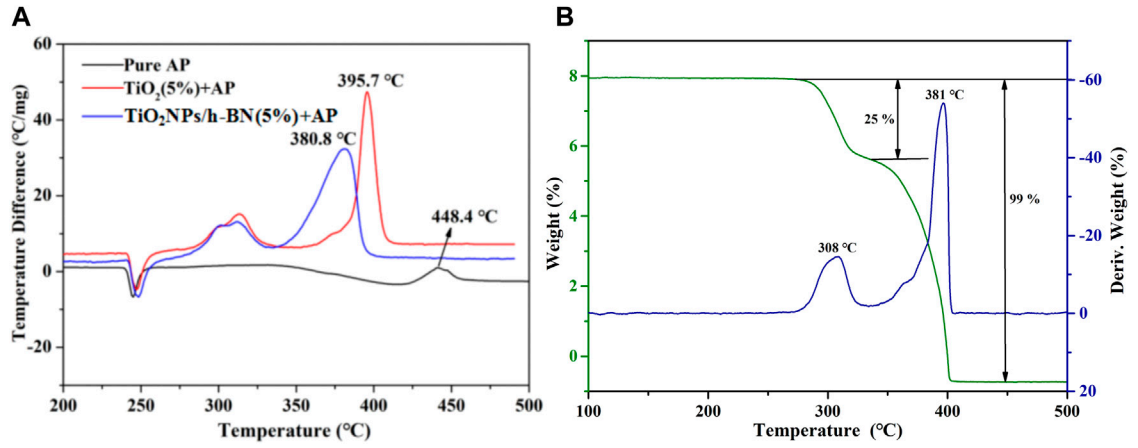

FIGURE 6
(A) DTA curves of pure AP; AP mixed with TiO_2 (5%); and AP mixed with TiO_2 NPs/h-BN (5%). **(B)** TG/DTG curves of AP mixed with TiO_2 NPs/h-BN (5%).

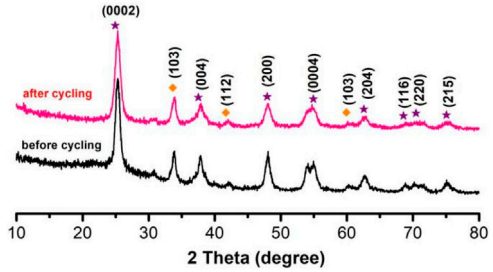

FIGURE 7
XRD of TiO_2 NPs/h-BN before and after thermal catalysis.

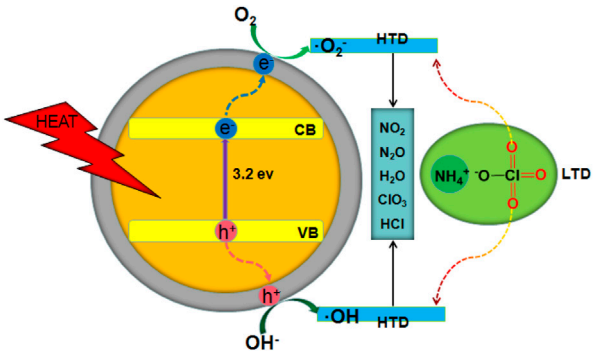

FIGURE 8
Schematic of the thermal decomposition of AP with TiO_2 NPs/h-BN as additives; CB, conduction band; VB, valence band.

TABLE 1 Recycling and stability of TiO_2 NPs/h-BN.

Cycle	Recovery rate	Decomposition temperature of AP (°C)
1	98 (%)	380.8
2	95 (%)	380.3
3	92 (%)	380.7

initiated subsequent surface degradation reaction (Li et al., 2008; Sharma et al., 2014; Eslami et al., 2017).

The catalytic process is shown in Figure 8. The adsorption of $HClO_4$ and NH_3 obtained from the first decomposition prevented the decomposition of AP. (Reid et al., 2007; Li et al., 2015a; Li et al., 2015b; Abazari and Mahjoub, 2017). As the temperature increased, conduction band electrons and valence band holes were generated on the surface of h-BN, and the generated electrons reacted with $HClO_4$, resulting in the reduction of $HClO_4$ to a superoxide radical anion. O_2^- further reacted with NH_3 to generate H_2O, NO_2, and N_2O (Zhang et al., 2014; Jain et al., 2019).

Conclusion

A novel TiO_2 NPs/h-BN hybrid material with strong interfacial interactions has been successfully constructed by *in situ* solvothermal growth. Experiments showed that the TiO_2 NPs/h-BN exhibited a good catalytic effect on the decomposition of AP, which reduced the high thermal decomposition temperature of AP by 67.6°C. At the same time, we deeply

analyzed TiO_2 NPs/h-BN as a novel catalyst to provide a mechanism for thermal decomposition of AP.

Data availability statement

The original contributions presented in the study are included in the article/Supplementary Material; further inquiries can be directed to the corresponding author.

Author contributions

JZ was responsible for the design of the test scheme, and DN was responsible for the writing of the manuscript.

Conflict of interest

The authors declare that the research was conducted in the absence of any commercial or financial relationships that could be construed as a potential conflict of interest.

Publisher's note

All claims expressed in this article are solely those of the authors and do not necessarily represent those of their affiliated organizations, or those of the publisher, the editors, and the reviewers. Any product that may be evaluated in this article, or claim that may be made by its manufacturer, is not guaranteed or endorsed by the publisher.

References

Abazari, R., and Mahjoub, A. R. (2017). Potential applications of magnetic β-AgVO3/ZnFe2O4 nanocomposites in dyes, photocatalytic degradation, and catalytic thermal decomposition of ammonium perchlorate. *Ind. Eng. Chem. Res.* 56, 623–634. doi:10.1021/acs.iecr.6b03727

Al-Ani, S. K. J., and Hogarth, C. A. (1985). Int.A study of optical absorption in tellurite and tungsten-tellurite glasses. *J. Electron.* 58, 123

Al-Kuhaili, M. F., Durrani, S. M. A., Khawaja, E. E., and Shirokoff, J. (2002). Effects of preparation conditions on the optical properties of thin films of tellurium oxide. *J. Phys. D. Appl. Phys.* 35, 312–915. doi:10.1088/0022-3727/35/9/312

Cui, X. Q., Zhao, Y. H., and Chu, Y. Q. (2012). The large sky area multi-object fiber spectroscopic telescope (LAMOST). *Res. Astronomy Astrophysics* 12, 1197. doi:10.1117/12.319250

Eslami, A., Juibari, N. M., Hosseini, S. G., and Abbasi, M. (2017). Synthesis and Characterization of CuO nanoparticles by the chemical liquid deposition method and investigation of its catalytic effect on the thermal decomposition of ammonium perchlorate. *Cent. Eur. J. Energy Mat.* 14, 152–168. doi:10.22211/cejem/67560

Hosseini, S. G., Zarei, M. A., Toloti, S. J. H., Kardan, H., and Alavi, M. A. (2018). A facile synthesis of boron nanostructures and investigation of their catalytic activity for thermal decomposition of ammonium perchlorate particles. *J. Therm. Anal. Calorim.* 131, 925–935. doi:10.1007/s10973-017-6595-7

Huang, T., Hao, W. J., Jin, B., Zhang, J. H., Guo, J. K., Luo, L. Q., et al. (2021). Novel energetic coordination compound [Cu (AT) $_4$] Cl_2 for catalytic thermal decomposition of ammonium perchlorate. *J. Solid State Chem.* 304, 122622. doi:10.1016/j.jssc.2021.122622

Huang, Y., Chen, D., Hu, X., Qian, Y., and Li, D. (2018). Synthesis and characterization of "ravine-like" BCN compounds with high capacitance. *Materials* 8, 209. doi:10.3390/ma11020209

Jacobs, P. W. M., and Russell-Jones, A. (1968). Sublimation of ammonium perchlorate. *J. Phys. Chem.* 72, 202–207. doi:10.1021/j100847a038

Jain, S., Khire, V. H., and Kandasubramanian, B. (2019). Barium titanate: a novel perovskite oxide burning rate modifier for HTPB/AP/Al based composite propellant formulations. Pune: Propellants, Explosives, Pyrotechnics.

Lei, L., Kong, T., Zhu, P., Kang, Z., Tian, X., Wang, L., et al. (2018). Self-assembly of TiO_2 nanofiber-based microcapsules by spontaneously evolved multiple emulsions. *Langmuir* 34, 8785–8791. doi:10.1021/acs.langmuir.8b01472

Li, H., Wu, C., Li, Y., and Zhang, J. (2012). Superior activity of MnOx-CeO_2/TiO_2 catalyst for catalytic oxidation of elemental mercury at low flue gas temperatures. *Appl. Catal. B Environ.* 111, 381–388. doi:10.1016/j.apcatb.2011.10.021

Li, K., Lei, Y., Liao, J., and Zhang, Y. (2021). Facile synthesis of MXene-supported copper oxide nanocomposites for catalyzing the decomposition of ammonium perchlorate. *Inorg. Chem. Front.* 8, 1747–1761. doi:10.1039/d0qi01337d

Li, K., Wang, B., Bolatibieke, D., Nan, D. H., and Li, Q. (2020). Pyrolysis of biomass impregnated with ammonium dihydrogen phosphate for polygeneration of phenol and supercapacitor electrode material. *Front. Chem.* 8, 436. doi:10.3389/fchem.2020.00436

Li, L., Sun, X., Qiu, X., Xu, J., and Li, G. (2008). Nature of catalytic activities of CoO nanocrystals in thermal decomposition of ammonium perchlorate. *Inorg. Chem.* 47, 8839–8846. doi:10.1021/ic8008283

Li, Q., He, Y., and Peng, R. (2015). Graphitic carbon nitride (g-C_3N_4) as a metal-free catalyst for thermal decomposition of ammonium perchlorate. *RSC Adv.* 5, 24507–24512. doi:10.1039/c5ra01157d

Li, Q., He, Y., and Peng, R. (2015). One-step synthesis of SnO_2 nanoparticles-loaded graphitic carbon nitride and their application in thermal decomposition of ammonium perchlorate. *Eur. J. Inorg. Chem.* 24, 4062–4067. doi:10.1002/ejic.201500507

Li, S. J., Chen, J. L., Hu, S. W., Wang, H. L., Chen, X. B., et al. (2020). Facile construction of novel Bi_2WO_6/Ta_3N_5 Z-scheme heterojunction nanofibers for efficient degradation of harmful pharmaceutical pollutants. *Chem. Eng. J.* 402, 126165. doi:10.1016/j.cej.2020.126165

Li, S. J., Hu, S. W., Jiang, W., Zhang, J. L., Xu, K. X., Wang, Z. H., et al. (2019). *In situ* construction of WO_3 nanoparticles decorated Bi_2MoO_6 microspheres for boosting photocatalytic degradation of refractory pollutants. *J. colloid interface Sci.* 556, 335–344. doi:10.1016/j.jcis.2019.08.077

Li, S. J., Hu, S. W., Jiang, W., Zhou, Y. T., Liu, J. S., and Wang, Z. H. (2018). Facile synthesis of cerium oxide nanoparticles decorated flower-like bismuth molybdate for enhanced photocatalytic activity toward organic pollutant degradation. *J. colloid interface Sci.* 530, 171–178. doi:10.1016/j.jcis.2018.06.084

Li, S. J., Shen, X. F., Liu, J. S., and Zhang, L. S. (2017). Synthesis of Ta_3N_5/Bi_2MoO_6 core-shell fiber-shaped heterojunctions as efficient and easily recyclable photocatalysts. *Environ. Sci. Nano* 4, 1155–1167. doi:10.1039/c6en00706f

Li, S. J., Wang, C. C., Chen, J. L., Zhang, P., Li, X., and Chen, X. B. (2022). Facile fabrication of TaON/Bi2MoO6 core–shell S-scheme heterojunction nanofibers for boosting visible-light catalytic levofloxacin degradation and Cr (VI) reduction. *Chem. Eng. J.* 428, 131158. doi:10.1016/j.cej.2021.131158

Li, S. J., Wang, C. C., Liu, Y. P., Xue, B., Chen, J. L., Wang, H. W., et al. (2020). Facile preparation of a novel Bi_2WO_6/calcined mussel shell composite photocatalyst with enhanced photocatalytic performance. *Catalysts* 10, 1166. doi:10.3390/catal10101166

Medvecká, V., Kováčik, D., Zahoranová, A., and Černák, M. (2018). Atmospheric pressure plasma assisted calcination by the preparation of TiO_2 fibers in submicron scale. *Appl. Surf. Sci.* 428, 609–615. doi:10.1016/j.apsusc.2017.09.178

Morales-Verdejo, C., Camarada, M. B., Arroyo, J. L., Povea, P., Carreño, G., Manriquez, J. M., et al. (2018). Effect of the homo- and heterobimetallic compounds derived from s-indacene on the thermal decomposition of ammonium perchlorate. *J. Therm. Anal. Calorim.* 131, 353–361. doi:10.1007/s10973-017-6534-7

Reid, D. L., Russo, A. E., Carro, R. V., Stephens, M. A., LePage, A. R., and Spalding, T. C. (2007). Nanoscale additives tailor energetic materials. *Nano Lett.* 7, 2157–2161. doi:10.1021/nl0625372

Sharma, J. K., Srivastava, P., and Singh, G. (2014). Nanocatalysts: Potential burning rate modifier for composite solid propellants. *Mat. focus* 3, 81–91. doi:10.1166/mat.2014.1154

Shen, G., Chen, D., and Lee, C. J. (2006). Hierarchical saw-like ZnO nanobelt/ZnS nanowire heterostructures induced by polar surfaces. *J. Phys. Chem. B* 110, 15689–15693. doi:10.1021/jp0630119

Shen, X. F., Yang, J. Y., Zheng, T., Wang, Q., Zhuang, H. F., Zheng, R. N., et al. (2020). Plasmonic pn heterojunction of $Ag/Ag_2S/Ag_2MoO_4$ with enhanced vis-NIR photocatalytic activity for purifying wastewater. *Sep. Purif. Technol.* 251, 117347. doi:10.1016/j.seppur.2020.117347

Shen, X. F., Zhang, Y., Shi, Z., Shan, S. D., Liu, J. S., Zhang, L. S., et al. (2021a). Construction of C_3N_4/CdS nanojunctions on carbon fiber cloth as a filter-membrane-shaped photocatalyst for degrading flowing wastewater. *J. Alloys Compd.* 851, 156743. doi:10.1016/j.jallcom.2020.156743

Shen, X. F., Yan, Z., Song, B. B. T., Chen, F., Xue, Q. Q., Shan, S. D., et al. (2021b). Magnetically recyclable and remarkably efficient visible-light-driven photocatalytic hexavalent chromium removal based on plasmonic biochar/bismuth/ferroferric oxide heterojunction. *J. Colloid Interface Sci.* 590, 424–435. doi:10.1016/j.jcis.2021.01.095

Sun, J., Lu, C., Song, Y., Ji, Q., Song, X., Li, Q., et al. (2018). *Recent progress in the tailored growth of two-dimensional hexagonal boron nitride via chemical vapour deposition*. Su zhou: Chemical Society Reviews.

Sun, W., Meng, Y., Fu, Q., Wang, F., Wang, G., Gao, W., et al. (2016). High-yield production of boron nitride nanosheets and its uses as a catalyst support for hydrogenation of nitroaromatics. *ACS Appl. Mat. Interfaces* 8, 9881–9888. doi:10.1021/acsami.6b01008

Thomas, A., Fischer, A., Goettmann, F., Antonietti, M., Müller, J. O., and Schlögl, R. (2008). Graphitic carbon nitride materials: variation of structure and morphology and their use as metal-free catalysts. *J. Mat. Chem.* 18, 4893. doi:10.1039/b800274f

Thomas, J. C., Demko, A. R., T, E., Reid, D. L., Seal, S., and Petersen, E. L. (2016). Mechanical properties of composite AP/HTPB propellants containing novel titania nanoparticles. *Prop. Explos. Pyrotech.* 41, 822–834. doi:10.1002/prep.201600090

Tu, D., Xu, C. N., Fujio, Y., Kamimura, S., Sakata, Y., and Ueno, N. (2014). Phosphorescence quenching by mechanical stimulus in CaZnOS: Cu. *Appl. Phys. Lett.* 105, 011908. doi:10.1063/1.4890112

Wang, X., Hu, W., and Hu, Y. (2020). Polydopamine-bridged synthesis of ternary h-BN@ PDA@ TiO_2 as nanoenhancers for thermal conductivity and flame retardant of polyvinyl alcohol. *Front. Chem.* 8, 587474. doi:10.3389/fchem.2020.587474

Xu, J., Zhang, L., Shi, R., and Zhu, Y. (2013). Chemical exfoliation of graphitic carbon nitride for efficient heterogeneous photocatalysis. *J. Mat. Chem. A Mat.* 1, 14766. doi:10.1039/c3ta13188b

Xue, J., Sanchez-Yamagishi, J., Bulmash, D., Jacquod, P., Deshpande, A., Watanabe, K., et al. (2011). Scanning tunnelling microscopy and spectroscopy of ultra-flat graphene on hexagonal boron nitride. *Nat. Mat.* 10, 282–285. doi:10.1038/nmat2968

Yuan, Y. J., Yang, Y., Li, Z., Chen, D., Wu, S., Fang, G., et al. (2018). Promoting charge separation in g-C_3N_4/graphene/MoS_2 photocatalysts by two-dimensional nanojunction for enhanced photocatalytic H_2 production. *ACS Appl. Energy Mat.* 1, 1400–1407. doi:10.1021/acsaem.8b00030

Zhang, J., Zhang, M., Yang, C., and Wang, X. (2014). Nanospherical carbon nitride frameworks with sharp edges accelerating charge collection and separation at a soft photocatalytic interface. *Adv. Mat.* 26, 4121–4126. doi:10.1002/adma.201400573

Zhao, J., Jin, B., Peng, R., Liu, Q., Tan, B., and Chu, S. (2016). Synthesis and characterization of a new energetic salt 1H-pyrazole-1-carboxamidine dinitramide and its thermal properties. *J. Therm. Anal. Calorim.* 124, 1431–1439. doi:10.1007/s10973-016-5315-z

Zhu, W., Gao, X., Li, Q., Li, H., Chao, Y., Li, M., et al. (2016). Controlled gas exfoliation of boron nitride into few-layered nanosheets. *Angew. Chem. Int. Ed. Engl.* 55, 10924–10928. doi:10.1002/ange.201605515